ROME
MeMeA 2018

JUNE 11-13, 2018

2018 IEEE International Symposium on Medical Measurements & Applications

memea2018.ieee-ims.org

- Welcome Message
- Table of Contents
- Technical Papers
- Authors Index

2018 SYMPOSIUM PROCEEDINGS

SPONSORS AND ORGANIZERS

IEEE INSTRUMENTATION & MEASUREMENT SOCIETY®

IEEE Advancing Technology for Humanity

ISBN: CFP18MEA-USB
Part Number: 978-1-5386-3391-5

Technical Support
Conference Catalysts
Phone: +1 352 872 5544
cdyer@conferencecatalysts.com

Technical Papers Table of Contents
Tuesday, June 12, 2018

11:30 – 13:10
T6.2: Measurements in medical imaging (II)
Room: Aula 1

This full text paper was peer-reviewed at the direction of IEEE Instrumentation and Measurement Society prior to the acceptance and publication.

Design and Experimental Test of a Microwave System for Quantitative Biomedical Imaging

Manuela Maffongelli, Samuel Poretti, Andrea Salvadè, Ricardo Monleone and Claudio Pagnamenta
Department of Technology and Innovation
University of Applied Sciences of Southern Switzerland
Manno, Switzerland
e-mail: {manuela.maffongelli; samuel.poretti; andrea.salvade; ricardo.monleone; claudio.pagnamenta}@supsi.ch

Alessandro Fedeli, Matteo Pastorino, and Andrea Randazzo
Department of Electrical Electronic, Telecommunication Engineering, and Naval Architecture
University of Genoa
Genova, Italy
e-mail: {alessandro.fedeli; matteo.pastorino; andrea.randazzo}@unige.it

***Abstract*—Despite the numerous advancements in the field of microwave measurement systems and techniques for biomedical and industrial applications, the development of cheap and reliable microwave imaging devices is still a challenge. In this contribution, a tomograph prototype specifically designed for medical imaging is presented. An array of custom antennas is placed in contact with the target, and the scattered field data are collected by means of a computer-controlled switching board connected to a vector network analyzer. The acquired data are then processed with a combined qualitative/quantitative inversion scheme, whose final goal is to retrieve a spatial map of the dielectric properties of the sample. After the description of the developed system and an outline of the adopted inversion method, preliminary experimental results are shown in order to validate the effectiveness of the approach.**

Keywords—microwave systems; nonlinear inversion, biomedical applications

I. INTRODUCTION

In the last years, there has been a growing interest in using microwave imaging techniques in biomedical applications, for both therapy and diagnostics [1]–[10]. In general, microwave imaging systems are composed by some radiating elements used to "illuminate" the body under test and one or more receiving elements able to collect the field scattered by the body. Since microwaves can penetrate inside dielectric materials, information concerning the internal structure of the body under test can be retrieved from the measured scattered-field data.

Biological bodies are however difficult to inspect at microwave frequencies since they are highly inhomogeneous, lossy, and dispersive structures. As a result, the signal is significantly attenuated during the propagation and, due to multiple reflections, the information about the material is contained in a complex way into the field that can be measured by the probes. Despite such difficulties, microwave imaging techniques can directly provide the maps of the dielectric parameters (i.e. the dielectric permittivity and the electric conductivity), which is a feature that cannot be obtained by using more consolidated diagnostic techniques, such as X-rays or ultrasounds. To this end, proper data processing algorithms should be used for retrieving the distributions of the dielectric properties of the target under test from the measured data. As it is well known, they are based on the solution of an inverse scattering problem, which suffers from two serious difficulties. First of all, it is strongly nonlinear. Moreover, it is also severely ill-posed. Therefore, particular care must be devoted to the development of the inversion algorithms, which have to provide a regularized solution and should avoid to be trapped in local minima, resulting in artefacts in the final image.

In summary, using microwaves for diagnostic applications is a very challenging problem. In the last years, the research in this field has been mainly focused on breast and brain stroke imaging. Both these applications have been addressed by using imaging apparatuses specifically designed and realized [11]–[17]. Actually, they must exhibit a very high dynamic range, since the field levels, in a noisy environment, are very low. Another problem is related to the need for the accurate knowledge of the incident field, i.e. the field which is present without the target. Such information is necessary not only at the measurement points, but also inside the "investigation" domain, which is the test region, usually located inside a plastic or metallic imaging chamber. Concerning the inversion procedures, in the field of breast and brain stroke imaging, both qualitative [18]–[22] and quantitative procedures [23]–[27] have been used to obtain the dielectric reconstructions. In the first case, the aim is to retrieve only the locations, the dimensions, or some other features of the discontinuities present inside the bodies. These discontinuities may be represented, for instance, by a tumor in the breast, blood in hemorrhagic stroke, or a necrotic mass in the ischemic stroke. On the contrary, quantitative procedures are aimed at reconstructing the complete distributions of the dielectric properties inside the target. This information can be directly related to the presence of dielectric discontinuities, allowing a direct observation of the effects of the pathology. Usually, quantitative procedures are more expensive from a computational point of view, which results in longer times for a complete diagnosis.

In this paper, a prototype of an imaging system, equipped with a set of custom antennas specifically developed for biomedical applications, is presented. A hybrid inversion algorithm, which combines a qualitative and a quantitative inversion procedure, is applied to estimate the distributions of the dielectric properties of the region of interest. In particular, the data collected by the tomograph prototype are firstly processed by means of a delay-and-sum radar-based method [4], [21], in order to produce a qualitative reconstruction of the target. After that, a Gauss-Newton inversion algorithm [28]–[32], which is able to exploit the information found in the qualitative step, is adopted to obtain the full distributions of the dielectric properties [33].

The paper is organized as follows. In Section II, the various parts of tomographic imaging system are described, whereas Section III outlines the developed nonlinear inversion algorithm. The experimental setup and some preliminary results are then reported in Section IV. Conclusions follow.

II. Automated Tomograph

The developed imaging system is based on a fully automated tomograph prototype intended for breast or other in-vivo tissues analysis. Fig. 1 shows the block diagram of the system. A personal computer (PC) is in charge of managing the active antenna pair, set/get vector network analyser (VNA) measurements, and run the reconstruction algorithms. The switching control board and the RF switch boards have been specifically designed in order to allow to independently drive 16 antennas located around the inspected target.

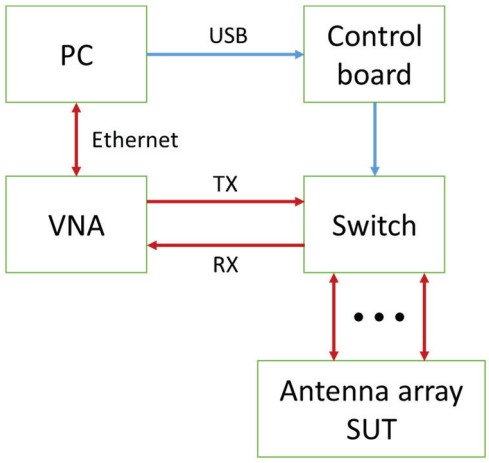

Fig. 1. Block diagram of the automated tomograph prototype.

A. Antenna array

An array composed by 16 antennas is used to illuminate the sample under test (SUT) and to collect the scattered electric field data. In order to avoid strong signal reflections due to the mismatch between the antennas and the SUT and to optimize the microwave propagation inside the inspected area, ad-hoc antennas have been specifically designed. They are *folded quasi self complementary antennas* (FQSCA) [34]. Such antennas allow operating directly in contact with the SUT, maintaining a reasonable operating bandwidth from 1.5 GHz up to 6 GHz and having the main lobe in the direction of the analyzed object.

The antennas are mounted on a plastic 3D printed frame (Fig. 6(*a*)). In particular, they are equally spaced on a circular ring of radius equal to 60 mm around the SUT with angular separation of 22.5°. The material used for the 3D prototype presents a relative dielectric constant ε_r of 2.97 and a loss tangent δ of 0.02 at 2.45 GHz. The effects of the plastic support have been preliminarily simulated by using commercial software based on the finite element method (FEM). The results of the simulations showed that the presence of this structure marginally affects the measured electric fields.

B. Switching board

The RF switching electronics has been developed to allow the 16 antennas to be independently commutated in order to obtain all the possible element pair combinations (240 couples). Each antenna can be used in transmitting (TX) or receiving (RX) mode. When a pair of antennas is used, the remaining 14 ones are left inactive thanks to the use of absorptive RF switch components. As described in [35], the use of terminations reduces the reflection of the signals received by inactive antennas in the array.

The switching network is composed by a combination of two different switching boards (1:4 and 2:4) as schematically shown in Fig. 2. Both topologies have been developed by using Peregrine Semiconductor's PE42441 SP4T absorptive RF switches able to operate in a frequency band from 10 MHz up to 8 GHz.

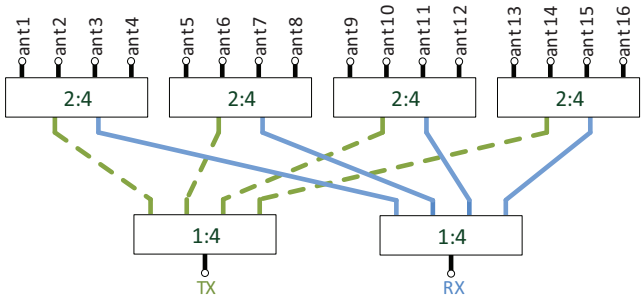

Fig. 2. Switching network block diagram.

In order to reduce the development time and ensure the same performances for all the boards, the same chip has been used for both switching parts (1:4 and 2:4). Fig. 3 shows the principle electrical schematics and a picture of the PCB of the developed 1:4 board. In order to reduce RF signal attenuation and electrical parameter variations, a Rogers RO4350B substrate has been used.

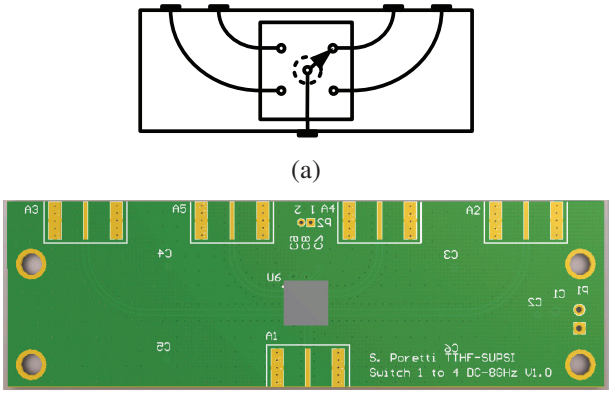

(a)

(b)

Fig. 3. (a) Switching board connection schematics and (b) picture of the developed PCB.

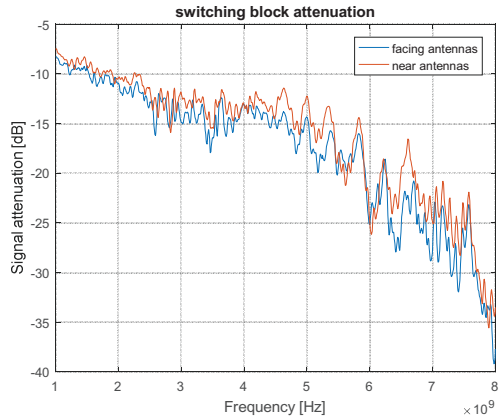

(a)

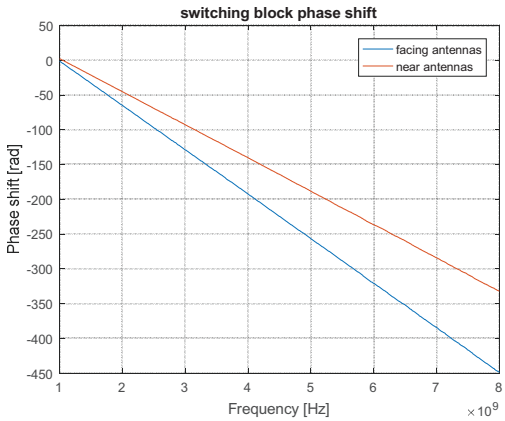

(b)

Fig. 4. Examples of the (a) attenuation and (b) phase shift introduced by the switching block.

The RF switching block is composed by several coaxial cables of different length. Also due to the different paths in the switching boards, signals are unevenly attenuated and phase shifted in function of the selected antenna pair. Fig. 4 shows two examples of the attenuations and phase shifts introduced by the switching block (for two different active antenna pairs). A calibration is therefore mandatory, in order to compensate both amplitude and phase variations due to the switching block and cables. In the present work, manual through measurement without antennas have been performed and saved for each combination. The corresponding attenuation and phase shift are then subtracted from the measurement with the SUT.

III. Reconstruction Algorithm

A combined qualitative-quantitative nonlinear inversion scheme has been adopted for processing the measured data, in order to obtain a reconstruction of the dielectric properties of the region of interest $\mathcal{D}$ (in the following denoted as *investigation domain*) in which the target is assumed to be located. The target is characterized by its relative dielectric permittivity $\varepsilon_r(\mathbf{r})$ and its electric conductivity $\sigma(\mathbf{r})$, with $\mathbf{r} \in \mathcal{D}$. Considering a known reference structure with relative dielectric permittivity $\varepsilon_{r,ref}(\mathbf{r})$ and electric conductivity $\sigma_{ref}(\mathbf{r})$ (e.g., an empty imaging chamber), the following contrast function can be defined

$$x(\mathbf{r}) = \varepsilon_r(\mathbf{r}) - \varepsilon_{r,ref}(\mathbf{r}) - j\frac{\sigma(\mathbf{r}) - \sigma_{ref}(\mathbf{r})}{\omega\varepsilon_0} \tag{1}$$

The data available for the inversion procedure, collected in the *observation domain* $\mathcal{O}$, are the measurements of the total field with the target $e_{tot}(\mathbf{r})$ and of the field due to the reference structure $e_{ref}(\mathbf{r})$, $\mathbf{r} \in \mathcal{O}$. The scattered field $e_{sc} = e_{tot} - e_{ref}$, is related to the contrast function x by a nonlinear relationship, i.e.,

$$\mathcal{N}(x) = e_{sc} \tag{2}$$

where $\mathcal{N}$ is the nonlinear scattering operator described in [33]. Since the problem of retrieving x (or, equivalently, ϵ_r and σ) given the scattered field e_{sc} is also ill-posed [36], a particular attention should be paid to the selection of proper inversion methods. In this work, a hybrid approach similar to the one proposed in [33] is tested for the first time for biomedical applications. As schematized in Fig. 5, it is based on the combination of a qualitative method with a quantitative inversion procedure. In more details, in the first step a delay-and-sum algorithm [4], [21] is used to produce a first qualitative tomographic image of the investigation domain $\mathcal{D}$, denoted as $\Lambda(\mathbf{r})$, $\mathbf{r} \in \mathcal{D}$. Subsequently, a quantitative Gauss-Newton inversion scheme is used, by taking advantage of the previously found qualitative map to focus the reconstruction in the regions of $\mathcal{D}$ in which the targets are located. The Gauss-Newton method iteratively performs a linearization of (2), obtaining, at the kth step, the linear equation

$$\mathcal{N}'_{x_k} h_k = e_{sc} - \mathcal{N}(x_k) \tag{3}$$

where x_k is the value of the unknown function x at the kth iteration, and $\mathcal{N}'_{x_k}$ is the Fréchet derivative of the operator $\mathcal{N}$ at x_k. Then, (3) is solved by using a regularizing truncated Landweber algorithm. After that, the solution h_k found in the inner Landweber loop, weighted by the qualitative map Λ, is utilized to update the unknown function as $x_{k+1} = x_k + \Lambda h_k$. Since the qualitative map has normalized values in the range between 0 and 1, all the cells of the investigation domain are iteratively updated, but the ones in which the delay-and-sum indicator function has found significant discontinuities with respect to the background (i.e. where Λ is close to 1) are weighted more than the others. In this way, the proposed algorithm allows to improve both the reconstruction accuracy and the computational efficiency.

In summary, the whole inversion method is structured as follows:

1. Retrieve a first qualitative map $\Lambda(\mathbf{r})$ of the investigation domain by applying the delay-and-sum algorithm [4].
2. Solve the nonlinear operator equation (2) by means of the iterative Gauss-Newton method (k indicates the iteration number), starting with an empty initial guess:
    a. Compute the first-order approximation of (2) around the current estimate of x (i.e., x_k), which leads to (3).
    b. Solve (3) by applying the regularizing truncated Landweber method, obtaining the increment h_k to be used to update the solution.
    c. Update the unknown function as $x_{k+1} = x_k + \Lambda h_k$ (Λ being the qualitative map found in step 1) and iterate from step a. until convergence is reached.

Additional details about the implementation of both the qualitative and quantitative steps of the proposed procedure can be found in [33].

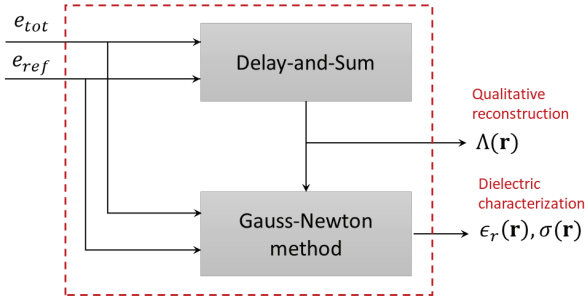

Fig. 5. Block scheme of the combined inversion procedure.

IV. Measurement Setup and Results

The preliminary tests of the proposed system have been carried out by considering the measurement configuration shown in Fig. 6. In particular, the target is composed by an outer Plexiglas cylinder of external diameter $d = 120$ mm, filled by a mixture of oil, water, and salt (relative dielectric permittivity $\epsilon_r \approx 7.4$, electric conductivity $\sigma \approx 0.7$ S/m at 2 GHz). The liquid mixture occupies a vertical depth of 90 mm. A plastic tube of diameter $d_i = 8$ mm, centered at $(x, y) = (-20, 20)$ mm, and filled with a different mixture of the same components (relative dielectric permittivity $\epsilon_r \approx 42$, electric conductivity $\sigma \approx 4.6$ S/m) has been also included.

The data acquired with the developed system have been processed by using the combined qualitative/quantitative method outlined in the previous Section. The investigation domain $\mathcal{D}$ has a circular cross section of diameter $d = 12$ cm, and it has been discretized into $N_{\mathcal{D}} = 1240$ square cells of side length 3.12 mm. The reference structure is the imaging chamber filled with a mixture of oil, water and salt, characterized by relative dielectric permittivity $\varepsilon_{r,ref} = 7.4$ and electric conductivity $\sigma_{ref} = 0.7$ S/m. The qualitative map of the investigation domain, which clearly shows the presence of the inclusion, is reported in Fig. 7. Moreover, Fig. 8 shows the reconstructed values of the relative dielectric permittivity at 1.9 GHz. As can be seen, the inclusion is correctly located and the dielectric properties of the inspected domain are retrieved with acceptable accuracy.

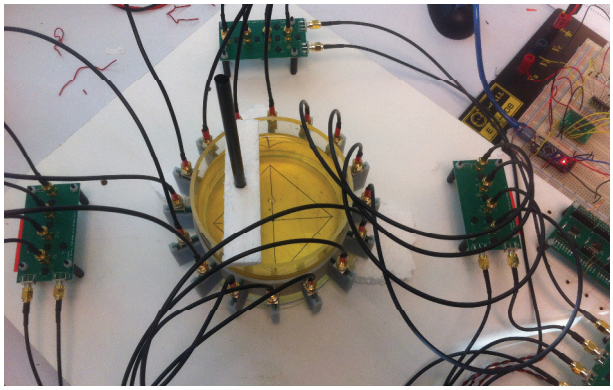

(a)

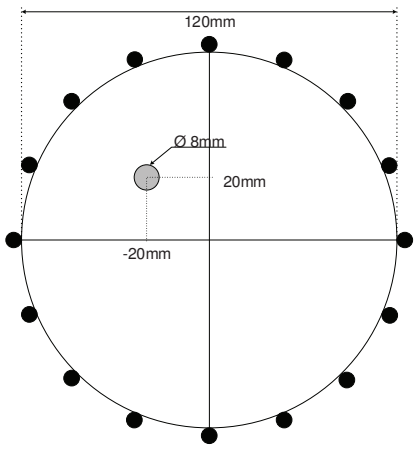

(b)

Fig. 6. Measurement configuration used to test the imaging prototype. (a) Photograph of the system. (b) Schematic representation of the target.

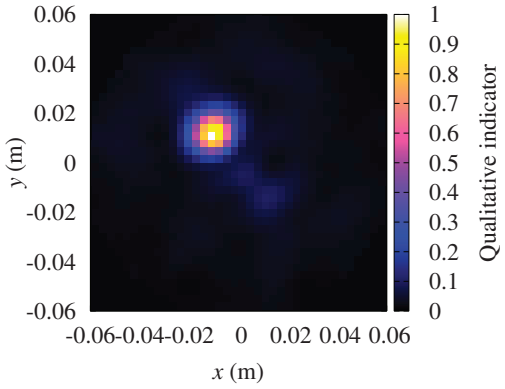

Fig. 7. Qualitative map provided by the first step of the inversion procedure.

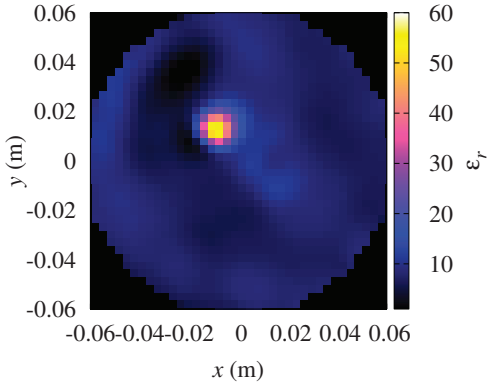

Fig. 8. Reconstructed distribution of the relative dielectric permittivity provided by quantitative inversion algorithm.

V. Conclusions

In this paper, a prototype of microwave imaging system for biomedical applications is presented. It is composed by an antenna array and a computer-controlled measurement apparatus that includes a vector network analyser and a switching block. The acquired data have been inverted by using a hybrid qualitative-quantitative reconstruction algorithm. Some preliminary experimental results, aimed at testing the functionalities of the system and at validating the effectiveness of the proposed inversion algorithm, have been reported. Further developments will include an extensive experimental validation in presence of more complex situations and realistic scenarios, involving inhomogeneous media, irregular shapes, and smooth discontinuities, as well as the extension to three-dimensional configurations.

References

[1] N. Nikolova, "Microwave imaging for breast cancer," *IEEE Microw. Mag.*, vol. 12, no. 7, pp. 78–94, Dec. 2011.

[2] E. C. Fear, P. M. Meaney, and M. A. Stuchly, "Microwaves for breast cancer detection?," *IEEE Potentials*, vol. 22, no. 1, pp. 12–18, Feb. 2003.

[3] Xu Li, E. J. Bond, B. D. Van Veen, and S. C. Hagness, "An overview of ultra-wideband microwave imaging via space-time beamforming for early-stage breast-cancer detection," *IEEE Antennas Propag. Mag.*, vol. 47, no. 1, pp. 19–34, Feb. 2005.

[4] R. C. Conceição, J. J. Mohr, and M. O'Halloran, Eds., *An Introduction to Microwave Imaging for Breast Cancer Detection*. Cham: Springer International Publishing, 2016.

[5] M. Persson *et al.*, "Microwave-based stroke diagnosis making global prehospital thrombolytic treatment possible," *IEEE Trans. Biomed. Eng.*, vol. 61, no. 11, pp. 2806–2817, Nov. 2014.

[6] D. Ireland and M. E. Bialkowski, "Microwave head imaging for stroke detection," *Prog. Electromagn. Res. M*, vol. 21, pp. 163–175, 2011.

[7] P.-H. Tournier *et al.*, "Numerical modeling and high-speed parallel computing: New perspectives on tomographic microwave imaging for brain stroke detection and monitoring," *IEEE Antennas Propag. Mag.*, vol. 59, no. 5, pp. 98–110, Oct. 2017.

[8] O. M. Bucci, M. Cavagnaro, L. Crocco, V. Lopresto, and R. Scapaticci, "Microwave ablation monitoring via microwave tomography: A numerical feasibility assessment," in *2016 10th European Conference on Antennas and Propagation (EuCAP)*, 2016, pp. 1–5.

[9] C. Gilmore, A. Zakaria, S. Pistorius, and J. LoVetri, "Microwave Imaging of Human Forearms: Pilot Study and Image Enhancement," *Int. J. Biomed. Imaging*, vol. 2013, Art. ID 673027, 2013.

[10] P. M. Meaney *et al.*, "Clinical Microwave Tomographic Imaging of the Calcaneus: A First-in-Human Case Study of Two Subjects," *IEEE Trans. Biomed. Eng.*, vol. 59, no. 12, pp. 3304–3313, Dec. 2012.

[11] M. Maffongelli, A. Salvadè, R. D. Monleone, S. Poretti, M. Pastorino, and A. Randazzo, "Microwave axial tomograph for medical applications: Preliminary set-up configuration," in *Proc. 2011 IEEE International Symposium on Medical Measurements and Applications (MeMeA)*, 2011, pp. 176–181.

[12] M. Maffongelli *et al.*, "Preliminary test of a prototype of microwave axial tomograph for medical applications," in *Proc. 2015 IEEE International Symposium on Medical Measurements and Applications (MeMeA)*, 2015, pp. 46–51.

[13] N. R. Epstein, P. M. Meaney, and K. D. Paulsen, "3D parallel-detection microwave tomography for clinical breast imaging," *Rev. Sci. Instrum.*, vol. 85, no. 12, Dec. 2014.

[14] D. Byrne, M. Sarafianou, and I. J. Craddock, "Compound radar approach for breast imaging," *IEEE Trans. Biomed. Eng.*, vol. 64, no. 1, pp. 40–51, Jan. 2017.

[15] E. C. Fear, J. Bourqui, C. Curtis, D. Mew, B. Docktor, and C. Romano, "Microwave Breast Imaging With a Monostatic Radar-Based System: A Study of Application to Patients," *IEEE Trans. Microw. Theory Techn.*, vol. 61, no. 5, pp. 2119–2128, May 2013.

[16] M. Hopfer, R. Planas, A. Hamidipour, T. Henriksson, and S. Semenov, "Electromagnetic tomography for detection, differentiation, and monitoring of brain stroke: A virtual data and human head phantom study," *IEEE Antennas Propag. Mag.*, vol. 59, no. 5, pp. 86–97, Oct. 2017.

[17] B. J. Mohammed, A. M. Abbosh, S. Mustafa, and D. Ireland, "Microwave System for Head Imaging," *IEEE Trans. Instrum. Meas.*, vol. 63, no. 1, pp. 117–123, Jan. 2014.

[18] D. Byrne, M. O'Halloran, M. Glavin, and E. Jones, "Data Independent Radar Beamforming Algorithms for Breast Cancer Detection," *Prog. Electromagn. Res.*, vol. 107, pp. 331–348, 2010.

[19] H. B. Lim, N. T. T. Nhung, E.-P. Li, and N. D. Thang, "Confocal Microwave Imaging for Breast Cancer Detection: Delay-Multiply-and-Sum Image Reconstruction Algorithm," *IEEE Trans. Biomed. Eng.*, vol. 55, no. 6, pp. 1697–1704, 2008.

[20] E. J. Bond, X. Li, S. C. Hagness, and B. D. Van Veen, "Microwave imaging via space-time beamforming for early detection of breast cancer," *IEEE Trans. Antennas Propag.*, vol. 51, no. 8, pp. 1690–1705, 2003.

[21] E. C. Fear, X. Li, S. C. Hagness, and M. A. Stuchly, "Confocal microwave imaging for breast cancer detection: localization of tumors in three dimensions," *IEEE Trans. Biomed. Eng.*, vol. 49, no. 8, pp. 812–822, 2002.

[22] A. Zamani, A. M. Abbosh, and S. Crozier, "Multistatic Biomedical Microwave Imaging Using Spatial Interpolator for Extended Virtual

Antenna Array," *IEEE Trans. Antennas Propag.*, vol. 65, no. 3, pp. 1121–1130, Mar. 2017.

[23] M. Ostadrahimi, P. Mojabi, A. Zakaria, J. LoVetri, and L. Shafai, "Enhancement of Gauss-Newton inversion method for biological tissue imaging," *IEEE Trans. Microw. Theory Techn.*, vol. 61, no. 9, pp. 3424–3434, Sep. 2013.

[24] L. M. Neira, B. D. Van Veen, and S. C. Hagness, "High-resolution microwave breast imaging using a 3-D inverse scattering algorithm with a variable-strength spatial prior constraint," *IEEE Trans. Antennas Propag.*, vol. 65, no. 11, pp. 6002–6014, Nov. 2017.

[25] P. Mojabi and J. LoVetri, "Microwave Biomedical Imaging Using the Multiplicative Regularized Gauss–Newton Inversion," *IEEE Antennas Wireless Propag. Lett.*, vol. 8, pp. 645–648, 2009.

[26] T. Rubek, P. M. Meaney, P. Meincke, and K. D. Paulsen, "Nonlinear Microwave Imaging for Breast-Cancer Screening Using Gauss–Newton's Method and the CGLS Inversion Algorithm," *IEEE Trans. Antennas Propag.*, vol. 55, no. 8, pp. 2320–2331, Aug. 2007.

[27] Z. Miao and P. Kosmas, "Multiple-frequency DBIM-TwIST algorithm for microwave breast imaging," *IEEE Trans. Antennas Propag.*, vol. 65, no. 5, pp. 2507–2516, May 2017.

[28] C. Estatico, M. Pastorino, and A. Randazzo, "An inexact-Newton method for short-range microwave imaging within the second-order Born approximation," *IEEE Trans. Geosci. Remote Sens.*, vol. 43, no. 11, pp. 2593–2605, Nov. 2005.

[29] G. Bozza, C. Estatico, M. Pastorino, and A. Randazzo, "An inexact Newton method for microwave reconstruction of strong scatterers," *IEEE Antennas Wireless Propag. Lett.*, vol. 5, no. 1, pp. 61–64, Dec. 2006.

[30] G. Oliveri, A. Randazzo, M. Pastorino, and A. Massa, "Electromagnetic imaging within the contrast-source formulation by means of the multiscaling inexact Newton method," *J. Opt. Soc. Am. A*, vol. 29, no. 6, pp. 945–958, May 2012.

[31] C. Estatico, M. Pastorino, and A. Randazzo, "A novel microwave imaging approach based on regularization in Lp Banach spaces," *IEEE Trans. Antennas Propag.*, vol. 60, no. 7, pp. 3373–3381, Jul. 2012.

[32] C. Estatico, A. Fedeli, M. Pastorino, and A. Randazzo, "A multifrequency inexact-newton method in Lp banach spaces for buried objects detection," *IEEE Trans. Antennas Propag.*, vol. 63, no. 9, pp. 4198–4204, Sep. 2015.

[33] F. Boero *et al.*, "Microwave Tomography for the Inspection of Wood Materials: Imaging System and Experimental Results," *IEEE Trans. Microw. Theory Techn.*, In print.

[34] M. Lanini, S. Poretti, A. Salvade, and R. Monleone, "Design of a slim wideband-antenna to overcome the strong reflection of the air-to-sample interface in microwave imaging," in *Proc. 2015 International Conference on Electromagnetics in Advanced Applications (ICEAA)*, Turin, Italy, 2015, pp. 1020–1023.

[35] S. Poretti, M. Lanini, A. Salvadè, M. Maffongelli, and R. Monleone, "Antenna design for microwave tomography imaging of high contrast mediums," in *2017 11th European Conference on Antennas and Propagation (EUCAP)*, 2017, pp. 1699–1702.

[36] M. Pastorino, *Microwave imaging*. Hoboken, N.J.: John Wiley & Sons, 2010.